RSC Advances

PAPER

View Article Online
View Journal | View Issue

Check for updates

Cite this: *RSC Adv.*, 2019, **9**, 24928

Controllable synthesis of $CsPbI_3$ nanorods with tunable photoluminescence emission

Zhikai Wen,[ab] Wei Zhai,[ab] Chang Liu,[ab] Jing Lin,*[ab] Chao Yu,*[ab] Yang Huang,*[ab] Jun Zhang[ab] and Chengchun Tang[ab]

Received 19th June 2019
Accepted 25th July 2019

DOI: 10.1039/c9ra04600c

rsc.li/rsc-advances

So far the controllable synthesis of one-dimensional (1D) $CsPbI_3$ nanocrystals still remains a challenge due to the fast reaction kinetics of the iodine system as compared with other halide perovskites. Here we report the direct synthesis of high-quality 1D $CsPbI_3$ nanorods by a facile solvothermal method. The as-prepared $CsPbI_3$ nanorods show high purity and uniform morphology with ultrafine diameters down to ~5 nm. By simply changing the solvothermal reaction conditions, fine-tuning of the sizes of the $CsPbI_3$ nanorods can be well achieved, which leads to the successful modulation of their photoluminescence (PL) emission. The solvothermal reaction offers relatively low crystal growth rate, which is of great importance for the size control of the $CsPbI_3$ nanocrystals. PL quantum yields (PLQYs) and lifetime results indicate that the obtained nanorods maintain a good surface state over long reaction time. Our work not only provides a reliable means for the synthesis of 1D iodine-related perovskites, but also expands the study of size-related PL properties on perovskites nanocrystals.

Open Access Article. Published on 12 August 2019. Downloaded on 6/18/2025 2:59:29 AM.
This article is licensed under a Creative Commons Attribution-NonCommercial 3.0 Unported Licence.

Introduction

In recent years, all-inorganic perovskite $CsPbX_3$ (X = Br, Cl, I) nanocrystals with high absorption coefficient,[1] high photoelectric conversion efficiency,[2] adjustable band gap,[3] high photoluminescence (PL) quantum yield (QY)[4] and better air stability[5] have shown high application value in the fields of semiconductor devices such as solar cells, light-emitting diodes, and photodetectors.[6–9] It is well known that perovskite nanocrystals have strong quantum confinement effects, and their PL characteristics are influenced by their morphology and size.[10–13] Among them, iodide perovskite nanocrystals have attracted great attention due to the unique narrow band gap and tunable efficient red emission.[14,15] More noteworthy is the one-dimensional (1D) $CsPbI_3$ nanocrystals with a particular crystallographic direction. Different from other structures and compositions of inorganic perovskite nanocrystals, 1D $CsPbI_3$ nanocrystals have fewer grain boundaries, limits carrier transport area and shortens the carrier transport distance, which provides conditions for the generation of high-efficiency optoelectronic devices.[16,17]

So far, many efforts have been developed for preparation of 1D $CsPbI_3$ nanocrystals. For example, Fang *et al.* synthesized $CsPbI_3$ nanorods with diameter of ~45 nm using a polar solvent controlled ionization method.[18] Zhang *et al.* used a solution-phase method to synthesize $CsPbI_3$ nanowires with tens to hundreds of diameters.[19] Recently, Chen *et al.* reported a two-step injection method for directly synthesizing $CsPbI_3$ nanowires with high stability.[20] In addition, the indirect synthesis of small-scale 1D $CsPbI_3$ nanocrystals (anion exchange,[21] chemical cutting[22]) has also received great attention. However, the development of simple and efficient direct synthesis of 1D $CsPbI_3$ nanocrystals with high purity and high quality is still challenging. In addition, the size control of the 1D $CsPbI_3$ nanocrystals can better meet the needs of semiconductor devices of different specifications.

Here, we use a simple solvothermal method to directly synthesize 1D $CsPbI_3$ nanorods with ultrafine diameter. The $CsPbI_3$ nanorods have high purity and narrow emission peak with a full width at half maxima (FWHM) of 29 nm. The strong quantum confinement effect allows the nanorods to achieve tunable size-dependent PL emission. Finally the PLQYs, PL lifetimes and stability are further studied.

Experimental

Preparation of PbI_2 precursor

2 mmol of PbI_2 and 20 mL of octadecene (ODE) were loaded into a 50 mL three-necked flask containing with 3 mL of oleic acid (OA) and 3 mL of oleylamine (OLA). The mixed solution was heated in an oil bath at 120 °C and kept under stirring until the PbI_2 salt was completely dissolved.

Preparation of Cs-oleate precursor

0.2 mmol of Cs_2CO_3, 18 mL of ODE and 2.5 mL of OA were added into a 50 mL three-necked flask. The solution was heated

[a]School of Materials Science and Engineering, Hebei University of Technology, Tianjin 300130, P. R. China. E-mail: linjing@hebut.edu.cn; yuchao20130426@126.com; huangyang@hebut.edu.cn
[b]Hebei Key Laboratory of Boron Nitride Micro and Nano Materials, Hebei University of Technology, Tianjin 300130, P. R. China

This journal is © The Royal Society of Chemistry 2019

Open Access Article. Published on 12 August 2019. Downloaded on 6/18/2025 2:59:29 AM.
This article is licensed under a Creative Commons Attribution-NonCommercial 3.0 Unported Licence.

in an oil bath at 125 °C and stirred constantly until all Cs_2CO_3 had reacted with OA. Then the solution was cooled down to room temperature.

Solvothermal synthesis of $CsPbI_3$ nanorods

In a typical experiment, 26 mL of PbI_2 precursor and 2 mL of Cs-oleate precursor were loaded into a Teflon lined autoclave (100 mL) at room temperature. The mixed solution was stirred for 3 min and then reacted at 100–180 °C for different times (1, 10, 40, 60, 90 min). After reaction, the crude solution was centrifuged at 10 000 rpm for 10 min to remove the residual reactants. The substrate was dispersed in 10 mL of *n*-hexane and centrifuged at 5000 rpm for 5 min to remove large particles.

Characterization

The crystallinity and morphology were measured by X-ray diffraction (XRD, BRUKER D8 DISCOVER) and transmission electron microscopy (TEM, Philips Tecnai F20 microscope). UV-Vis absorption spectra were collected using a Japan HITACHI U-3900H spectrometer. PLQY and lifetime measurements were performed by Fluorolog-3 Horiba Jobin-Yvon spectrofluorimeter equipped with an integrating sphere. The actual contents of metal loading were analyzed by inductively coupled plasma emission spectroscopy (ICP-AES, Optima 8300).

Results and discussion

The XRD pattern indicates that the prepared $CsPbI_3$ nanorods are crystallized in cubic phase (Fig. 1a). The main peaks of the samples are located at 14.3°, 20.3°, 28.8° and 32.2°, corresponding to the (100), (110), (200) and (201) planes of cubic $CsPbI_3$, respectively.[23,24] It is well known that $CsPbI_3$ is stable existence in the form of a orthorhombic phase at ambient temperature.[25] The presence of orthorhombic phase was not observed in the XRD pattern of our sample, demonstrating the high purity of the sample. Typical TEM image of the sample is shown in Fig. 1b. The product consists of numerous 1D rod-shaped nanoparticles. The nanorods have uniform morphology with average length of ~80 nm. Interestingly, all of the nanorods tend to arrange as regular arrays. In addition, no other impurities such as nanoparticles can be observed, illustrating the high purity and regular morphology of the product. High-resolution TEM (HRTEM) image of an individual nanorod (Fig. 1c) demonstrates that the nanorod has an ultrafine diameter of ~4.6 nm. The crystal structure of the sample can also been verified by HRTEM observation. The planes are perpendicular to the long axis of the nanorods and show an interplanar spacing of 0.31 nm, which can be attributed to the (200) plane of cubic $CsPbI_3$. So the nanorods should grow along [100] direction. Due to the small size and uniform morphology, the nanorods still have good dispersibility in hexane, which is undoubtedly advantageous for solution reprocessing and the measurement of optical properties of the samples.

The UV-Vis absorption and PL emission spectra of the $CsPbI_3$ nanorods are shown in Fig. 1d. The PL spectrum displays an emission peak centered at ~618 nm, which is consistent with the phenomenon that the sample emits visible bright red light in the light box irradiated by 365 nm ultraviolet light (shown in inset of Fig. 1d). As compared with bulk $CsPbI_3$ which often displays red emission at 710 nm,[26] here the PL emission with a blue shift of ~92 nm can be attributed to the strong quantum confinement effect in the ultrafine nanorods. In fact, the nanorods have diameters far below the Bohr radius (~6.5 nm) of $CsPbI_3$.[27] It is also noteworthy that the emission peak has a narrow full width at half maxima (FWHM) of only 29 nm, further confirming the high uniformity of the nanorods. Normally the synthesis of 1D $CsPbI_3$ nanocrystals may require higher temperatures with the aim of ensure the uniformity of sample size (Zhang synthesized $CsPbI_3$ nanowires at temperatures higher than 180 °C [19]), whereas our synthesis process can be carried out at a relatively low temperature, which should be attributed to the high pressure environment in the autoclave. The UV-Vis absorption peak is located at ~601 nm, and the nanorod has a typical Stokes shift of 13 nm.

The fine-tune on the morphology of the $CsPbI_3$ nanorods can be well achieved by simply changing the solvothermal reaction times (0–90 min). TEM images (Fig. 2a–d) indicate that the sizes of the samples change regularly. The sample obtained after 1 min's reaction (1 min after the reaction temperature rises to 160 °C) consists of nanorods with high aspect ratios and flexible feature (Fig. 2a). When the reaction time is extended to 90 min, the shape of the product gradually changes into straight and short nanorods (Fig. 2d). Statistical diagrams of the length and diameter distributions based on the statistics of more than 100 nanorods in each sample are shown in Fig. 2e–h. With an increase of reaction time, the average length of the sample decreases from ~264 to ~62 nm, while the diameter changes slightly from ~4.1 to ~5.1 nm. This indicates that the sizes of the $CsPbI_3$ nanorods can be fine controlled by changing the solvothermal reaction times. As compared with the obviously decrease in nanorod lengths, the slightly change in their diameter may be attributed to the 1D growth direction. In addition, all of the samples show well monodispersity with no obvious impurities. Even if the reaction is extended to 90 min, the sample maintains regular 1D morphology. The results indicate that the solvothermal conditions can effectively control the reaction rate between Cs-oleate and PbI_2 precursors. The sample in the reaction can be kept in a relatively stable state, and the generation of impurities can be suppressed.

It is noteworthy that iodine system always has faster reaction kinetics as compared with other halide pervoskites. However, the fast kinetics always result in larger diameters (tens or hundreds of nanometers). Therefore, the controllable synthesis of 1D $CsPbI_3$ nanocrystals still remains challenges. With the aim of controllable synthesis of $CsPbI_3$ nanocrystals, a relatively mild growth environment which can effectly suppress the reaction kinetics of iodine system is highly desirable. Our results have shown that ultrafine 1D $CsPbI_3$ nanocrystals with diameters of less than 10 nm can be successfully obtained by the solvothermal method and the sizes can be well tuned by adjusting the reaction times. The solvothermal reaction in the sealed environment offers relatively low crystal growth rate,

Open Access Article. Published on 12 August 2019. Downloaded on 6/18/2025 2:59:29 AM.
This article is licensed under a Creative Commons Attribution-NonCommercial 3.0 Unported Licence.

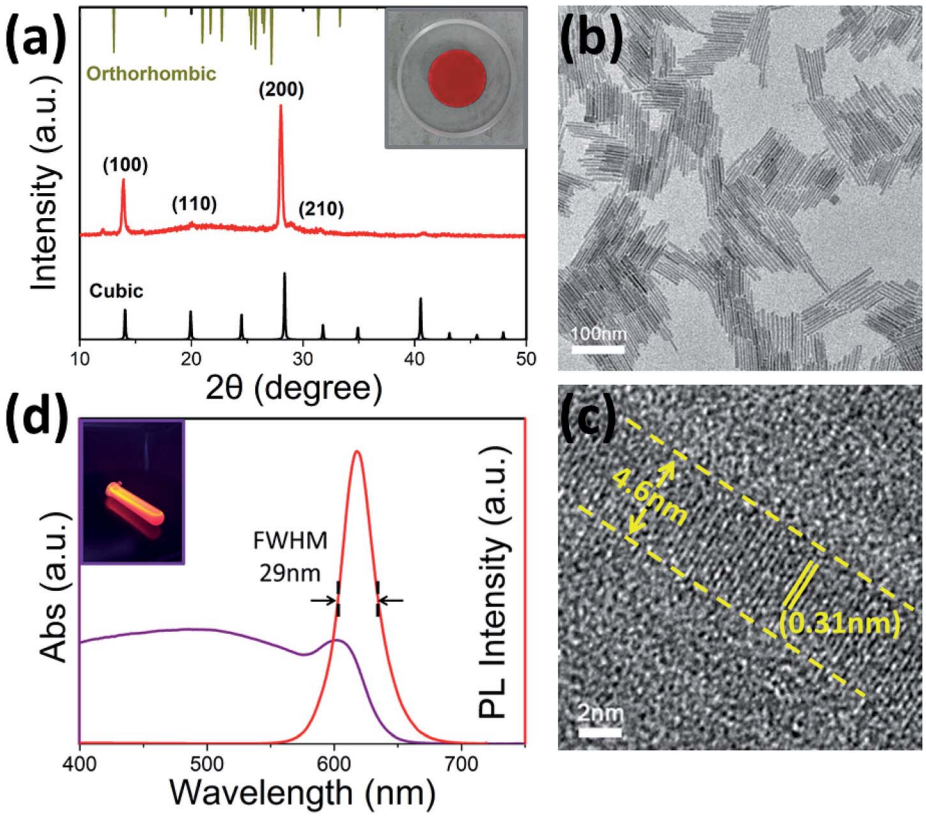

Fig. 1 XRD pattern (a) and TEM image (b) of the $CsPbI_3$ nanorods. Inset shows an optical picture of a high concentration of $CsPbI_3$ nanorods deposited directly on the sample stage. (c) HRTEM image of an individual nanorod. (d) UV-Vis absorption and PL emission spectra of the nanorods.

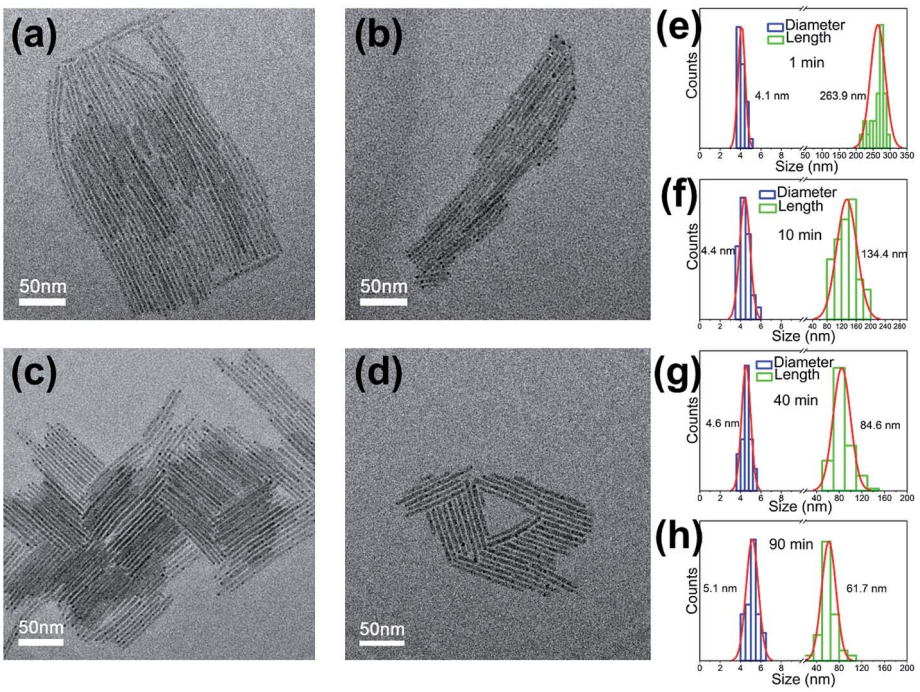

Fig. 2 TEM images of $CsPbI_3$ nanorods prepared at 1 min (a), 10 min (b), 40 min (c) and 90 min (d). (e–h) The corresponding diameter and length distribution histograms.

This journal is © The Royal Society of Chemistry 2019

Open Access Article. Published on 12 August 2019. Downloaded on 6/18/2025 2:59:29 AM.
This article is licensed under a Creative Commons Attribution-NonCommercial 3.0 Unported Licence.

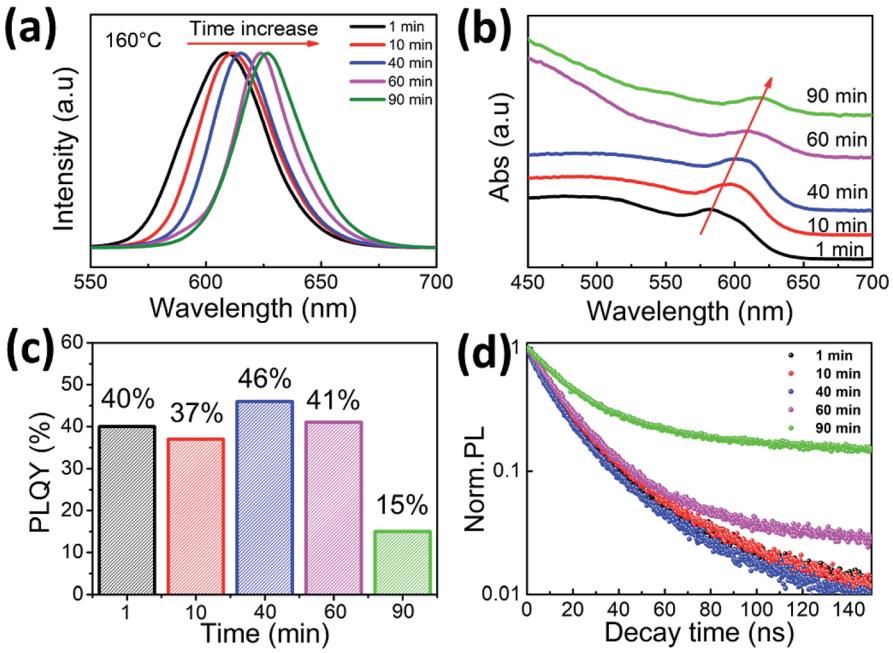

Fig. 3 PL emission spectra (a), UV-Vis absorption spectra (b), PLQYs (c) and time-resolved PL decay curves (d) of $CsPbI_3$ nanorods prepared at different times.

which is of great importance for the size control. It has also been experimentally proved that changes in external pressure will lead to changes in the band gap of the synthesized perovskite.[28] It is believed that the high pressure environment also plays an important role in the synthesis of $CsPbI_3$ nanocrystals. In addition, the role of the ligands cannot be ignored. In the reaction process, oleic acid and oleylamine as surface ligands can change the kinetic pathway, promote the formation of anisotropic nanostructures, and stabilize the final colloidal nanostructure.[29] Here, we used ICP to understand the amount of organic ligands in the sample. In detail, the $CsPbI_3$ nanorods with organic surfactants on surfaces were separated from *n*-hexane dispersion by ultracentrifugation and filtration and then weighted. Then the $CsPbI_3$ nanorods with organic surfactants on surfaces were redissolved in distilled water and the concentration of Pb^+ was measured by ICP-AES. Finally we could calculate the amount of organic surfactants in the samples. The mass ratio of $CsPbI_3$ nanocrystals to surface ligands is calculated to be $\sim$1 : 6. We believe that a relatively high amount of ligands is beneficial to inhibit the rapid growth of $CsPbI_3$ nanocrystals. Moreover, the proper ratio of oleic acid and oleylamine leads to the generation of 1D structure.

The as-prepared $CsPbI_3$ nanorods display distinct size-dependent PL properties. The PL emission peaks of samples prepared with an increasing reaction times show a significant red shift from 609 to 627 nm (Fig. 3a). The nanorods have diameters relative to the exciton Bohr diameters of $CsPbI_3$. Therefore, the tunable sizes of the nanorods is responsible for the red shift of PL emission due to the quantum confinement effect. Correspondingly, the absorption peaks of the nanorods also change from 585 nm to 619 nm (Fig. 3b). The PLQY is an important performance parameter for the luminescent materials. Fig. 3c shows the measured PLQYs of the samples prepared at different reaction times. The PLQYs of nanorods are 40%, 37%, 46%, 41%, and 15%, respectively. The PL decay curves of the as-prepared nanorods are shown in Fig. 3d. The average lifetimes of the different samples are 18, 16, 17, 20, and 32 ns, respectively. The lifetimes can be analyzed by double-exponential fitting method, as shown in Table 1. All of the average lifetimes contain short lifetime components (τ_1) and long lifetime components (τ_2). The long lifetimes are associated with non-radiative recombination, while the short lifetime components represent radiation recombination.[30] In our work, the sample obtained with short reaction time has a higher ratio of short lifetime component (A_1), indicating the fast radiation recombination rate and therefore has higher PLQYs. The luminescent properties of perovskite nanocrystal are also affected by the binding between it and the ligand.[31] Only when the reaction is extended to 90 min, the PLQY and lifetime of the nanorods show significant changes, which means that the obtained nanorods are able to maintain these properties stably over a relatively long reaction time in a solvothermal environment, thereby ensuring stable luminescence.

Table 1 The detailed recombination lifetimes described by double-exponential fitting method

$CsPbI_3$ sample	τ_1 (ns)	A_1 (%)	τ_2 (ns)	A_2 (%)	τ_{avg} (ns)
1 min	13.6	60.98	48	39.02	18
10 min	10.1	58.39	40.2	41.61	16
40 min	13.6	55.05	44	44.95	17
60 min	14.5	69.09	56.3	30.91	20
90 min	17.4	44.96	108	55.04	32

Open Access Article. Published on 12 August 2019. Downloaded on 6/18/2025 2:59:29 AM.
This article is licensed under a Creative Commons Attribution-NonCommercial 3.0 Unported Licence.

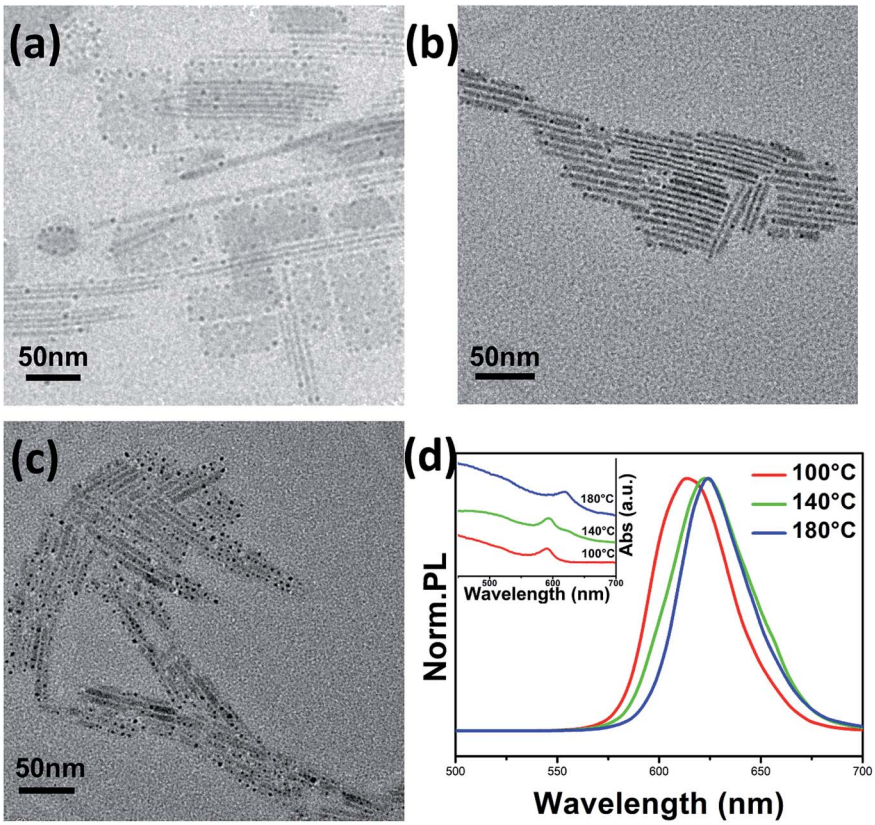

Fig. 4 TEM images of $CsPbI_3$ nanocrystals prepared at 100 °C (a), 140 °C (b), and 180 °C (c) for 1 h. (d) PL emission spectra and UV-Vis absorption spectra of the samples.

The size-dependent PL emission can also be achieved by controlling of the solvothermal reaction temperatures. Fig. 4a–c show typical TEM images of different samples prepared at temperatures from 100 °C to 180 °C, respectively. It should be noted that at lower temperature conditions (100 °C), both nanowires and nanosheets are present in the product, wherein the nanosheets have lateral sizes of 50–100 nm. As the temperature increased, the samples show higher purity with rodlike morphology (Fig. 4b and c), which means that in a solvothermal reaction, a higher temperature is advantageous for the 1D growth of the nanocrystals. In addition, some black spots were observed in our samples because the perovskite nanocrystals were not stable in the TEM test environment, especially after prolonged exposure. The structure of the perovskite is easily destroyed by the electron beam, which results in the production of a large number of lead points. Such

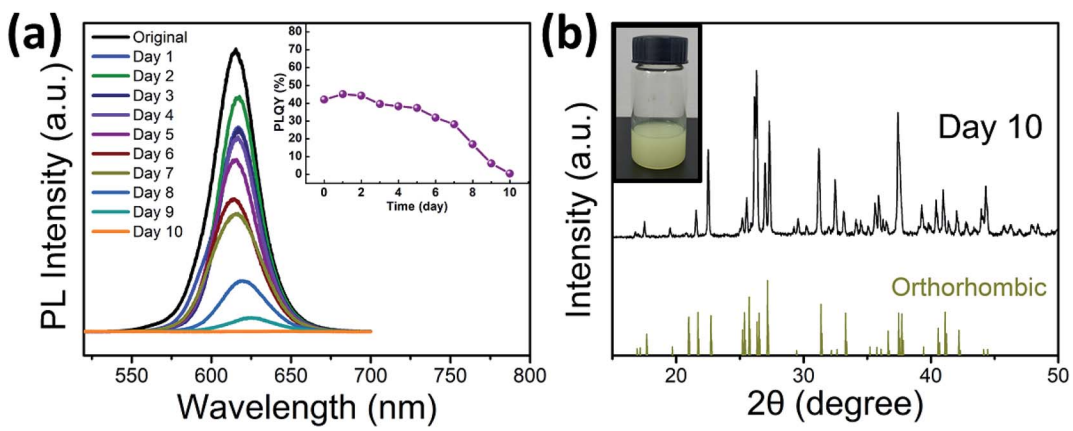

Fig. 5 (a) Change of the PL intensity and PLQY of the $CsPbI_3$ nanorods (prepared at 160 °C for 40 min) under ambient conditions *versus* storage time. (b) XRD pattern of the sample stored under ambient conditions for 10 days. The inset shows the optical picture after phase transition of the $CsPbI_3$ nanorods.

This journal is © The Royal Society of Chemistry 2019

Open Access Article. Published on 12 August 2019. Downloaded on 6/18/2025 2:59:29 AM.
This article is licensed under a Creative Commons Attribution-NonCommercial 3.0 Unported Licence.

phenomena have also been reported in the synthesis of other perovskites.[32] The PL properties of the products also change accordingly. As shown in Fig. 4d, the samples have tunable PL emission with a red shift from 613 to 624 nm. As compared with the red shift caused by the change of reaction time (~28 nm), here the narrower shift is due to the relative smaller size-change resulted by the change of reaction temperatures. Therefore, we believe that the changing of solvothermal reaction time without affecting the purity of the product is a more effective means of regulating the PL properties of the $CsPbI_3$ nanorods.

Finally, the stability of the as-prepared $CsPbI_3$ nanorods has also been evaluated. The PL emission spectra of the sample (prepared at 160 °C for 40 min) after stored in air for several days are shown in Fig. 5a. The PL intensity decreases slowly within the first 5 days, and the measured PLQY (shown inset of Fig. 5a) does not even have obvious attenuation. However, after 5 days, the decay rate of the PL intensity is obviously faster, and PLQY is also attenuated from 38% to 1%. In addition, a red shift of the emission peak (from 515 to 525 nm) can be observed, which may be due to particle size changes caused by agglomeration of the nanorods. XRD result (Fig. 5b) indicates that the cubic $CsPbI_3$ was converted to orthorhombic $CsPbI_3$ after 10 days of storage. The color of the sample also changes from red to pale yellow (inset of Fig. 5b). In addition to the normal temperature phase instability of cubic $CsPbI_3$, moisture in the air may also accelerate its structural changes.[20] Therefore, inert gas protection and proper packaging are necessary.

Conclusions

In summary, monodisperse and uniform-sized $CsPbI_3$ nanorods were synthesized by a solvothermal method. The controlled size adjustment can be achieved by changing the reaction time and temperatures, which provides a simple and feasible solution for the regulation on the morphology of perovskite nanocrystals, especially in the 1D direction. The narrow emission and adjustable PL properties indicate that the $CsPbI_3$ nanorods have good application potential in the field of luminescence. Our work not only expands the morphological study of perovskite nanocrystals, but also expands the study of its size-related PL properties.

Conflicts of interest

There are no conflicts to declare.

Acknowledgements

This work was supported by the National Natural Science Foundation of China (51572068, 51772075, 21806029), the Natural Science Foundation of Hebei Province (E2019202086, E2019202347), the Hundred Talents Program of Hebei Province (E2014100011), and the Program for Changjiang Scholars and Innovative Research Team in University (PCSIRT: IRT17R33).

Notes and references

1 J. De Roo, M. Ibáñez, P. Geiregat, G. Nedelcu, W. Walravens, J. Maes, J. C. Martins, I. Van Driessche, M. V. Kovalenko and Z. Hens, *ACS Nano*, 2016, **10**, 2071–2081.
2 H. Kim, J. S. Han, J. Choi, S. Y. Kim and H. W. Jang, *Small Methods*, 2018, **2**, 1700310.
3 H. Zhou, S. Yuan, X. Wang, T. Xu, X. Wang, H. Li, W. Zheng, P. Fan, Y. Li and L. Sun, *ACS Nano*, 2016, **11**, 1189–1195.
4 F. Liu, Y. Zhang, C. Ding, S. Kobayashi, T. Izuishi, N. Nakazawa, T. Toyoda, T. Ohta, S. Hayase and T. Minemoto, *ACS Nano*, 2017, **11**, 10373–10383.
5 J. S. Han, Q. Van Le, J. Choi, K. Hong, C. W. Moon, T. L. Kim, H. Kim, S. Y. Kim and H. W. Jang, *Adv. Funct. Mater.*, 2018, **28**, 1705783.
6 B. Li, Y. Zhang, L. Fu, T. Yu, S. Zhou, L. Zhang and L. Yin, *Nat. Commun.*, 2018, **9**, 1076.
7 Y. Tian, C. Zhou, M. Worku, X. Wang, Y. Ling, H. Gao, Y. Zhou, Y. Miao, J. Guan and B. Ma, *Adv. Mater.*, 2018, **30**, 1707093.
8 W. Zhai, J. Lin, C. Li, S. Hu, Y. Huang, C. Yu, Z. Wen, Z. Liu, Y. Fang and C. Tang, *Nanoscale*, 2018, **10**, 21451–21458.
9 Y. Wang, M. Yasar, Z. Luo, S. Zhou, Y. Yu, H. Li, R. Yang, X. Wang, A. Pan and L. Gan, *Small*, 2018, **14**, 1803010.
10 H. He, B. Tang and Y. Ma, *Nanotechnology*, 2018, **29**, 55601.
11 W. Zhai, J. Lin, Q. Li, K. Zheng, Y. Huang, Y. Yao, X. He, L. Li, C. Yu and C. Liu, *Chem. Mater.*, 2018, **30**, 3714–3721.
12 J. Song, J. Li, X. Li, L. Xu, Y. Dong and H. Zeng, *Adv. Mater.*, 2015, **27**, 7162–7167.
13 Y. Wu, X. Li and H. Zeng, *ACS Energy Lett.*, 2019, **4**, 673–681.
14 L. Martinez-Sarti, S. H. Jo, Y. H. Kim, M. Sessolo, F. Palazon, T. W. Lee and H. J. Bolink, *Nanoscale*, 2019, **11**, 12793–12797.
15 A. Dutta, S. K. Dutta, S. Das Adhikari and N. Pradhan, *Angew. Chem., Int. Ed.*, 2018, **57**, 9083–9087.
16 W. Tian, H. Zhou and L. Li, *Small*, 2017, **13**, 1702107.
17 T. Yang, Y. Zheng, Z. Du, W. Liu, Z. Yang, F. Gao, L. Wang, K. C. Chou, X. Hou and W. Yang, *ACS Nano*, 2018, **12**, 1611–1617.
18 F. Fang, W. Chen, Y. Li, H. Liu, M. Mei, R. Zhang, J. Hao, M. Mikita, W. Cao and R. Pan, *Adv. Funct. Mater.*, 2018, **28**, 1706000.
19 D. Zhang, S. W. Eaton, Y. Yu, L. Dou and P. Yang, *J. Am. Chem. Soc.*, 2015, **137**, 9230–9233.
20 Z. Chen, L. Dong, H. Tang, Y. Yu, L. Ye and J. Zang, *CrystEngComm*, 2019, **21**, 1389–1396.
21 D. Zhang, Y. Yang, Y. Bekenstein, Y. Yu, N. A. Gibson, A. B. Wong, S. W. Eaton, N. Kornienko, Q. Kong and M. Lai, *J. Am. Chem. Soc.*, 2016, **138**, 7236–7239.
22 Y. Tong, M. Fu, E. Bladt, H. Huang, A. F. Richter, K. Wang, P. Müller-Buschbaum, S. Bals, P. Tamarat and B. Lounis, *Angew. Chem.*, 2018, **130**, 16326–16330.
23 G. E. Eperon, G. M. Paterno, R. J. Sutton, A. Zampetti, A. A. Haghighirad, F. Cacialli and H. J. Snaith, *J. Mater. Chem. A*, 2015, **3**, 19688–19695.
24 P. Luo, W. Xia, S. Zhou, L. Sun, J. Cheng, C. Xu and Y. Lu, *J. Phys. Chem. Lett.*, 2016, **7**, 3603–3608.

Open Access Article. Published on 12 August 2019. Downloaded on 6/18/2025 2:59:29 AM.
This article is licensed under a Creative Commons Attribution-NonCommercial 3.0 Unported Licence.

25 Y. Zhou and Y. Zhao, *Energy Environ. Sci.*, 2019, **12**, 1495–1511.
26 C. C. Stoumpos, C. D. Malliakas and M. G. Kanatzidis, *Inorg. Chem.*, 2013, **52**, 9019–9038.
27 L. Protesescu, S. Yakunin, M. I. Bodnarchuk, F. Krieg, R. Caputo, C. H. Hendon, R. X. Yang, A. Walsh and M. V Kovalenko, *Nano Lett.*, 2015, **15**, 3692–3696.
28 Y. Cao, G. Qi, C. Liu, L. Wang, Z. Ma, K. Wang, F. Du, G. Xiao and B. Zou, *J. Phys. Chem. C*, 2018, **122**, 9332–9338.
29 A. Pan, B. He, X. Fan, Z. Liu, J. J. Urban, A. P. Alivisatos, L. He and Y. Liu, *ACS Nano*, 2016, **10**, 7943–7954.
30 X. Li, Y. Wu, S. Zhang, B. Cai, Y. Gu, J. Song and H. Zeng, *Adv. Funct. Mater.*, 2016, **26**, 2435–2445.
31 D. Yang, X. Li, W. Zhou, S. Zhang, C. Meng, Y. Wu, Y. Wang and H. Zeng, *Adv. Mater.*, 2019, 1900767.
32 Q. A. Akkerman, S. G. Motti, A. R. Srimath Kandada, E. Mosconi, V. D'Innocenzo, G. Bertoni, S. Marras, B. A. Kamino, L. Miranda and F. De Angelis, *J. Am. Chem. Soc.*, 2016, **138**, 1010–1016.

This journal is © The Royal Society of Chemistry 2019